



Horizon 2020
Programme

CORTEX

Research and Innovation Action (RIA)

This project has received funding from the European Union's Horizon 2020 research and innovation programme under grant agreement No 754316.

Start date : 2017-09-01 Duration : 48 Months
<http://cortex-h2020.eu>



Description of scenarios for the simulated data

Authors : Pr. Christophe DEMAZIERE (Chalmers), Abdelhamid Dokhane (PSI)

CORTEX - Contract Number: 754316

Core monitoring techniques and experimental validation and demonstration Foivos MARIAS

Document title	Description of scenarios for the simulated data
Author(s)	Pr. Christophe DEMAZIERE, Abdelhamid Dokhane (PSI)
Number of pages	30
Document type	Deliverable
Work Package	WP03
Document number	D3.1
Issued by	Chalmers
Date of completion	2019-02-13 17:02:30
Dissemination level	Public

Summary

This report summarizes the different scenarios corresponding to the presence of various noise sources in nuclear reactors. The definition of the noise sources and their modelling are carefully detailed, together with the modelling of their effect onto the neutron noise in a nuclear reactor core. Both frequency-domain and time-domain simulation strategies are presented. For the frequency-domain approach, the scenarios include: a generic "absorber of variable strength", axially-travelling perturbations at the velocity of the flow (due to e.g. fluctuations of the coolant temperature or coolant flow at the inlet of the core), fuel assembly vibrations, control rod vibrations, and core barrel vibrations. For the time-domain approach, the scenarios include: fuel assembly vibrations, inlet coolant temperature fluctuations, inlet coolant flow fluctuations, and their possible combinations.

Approval

Date	By
2019-02-27 23:44:03	Pr. Kollias STEFANOS (University of Lincoln)
2019-02-28 08:26:30	Pr. Christophe DEMAZIERE (Chalmers)

Table of Contents

1	Introduction	3
2	Prerequisites	3
2.1	Core instrumentation	3
2.2	Data required for frequency-domain simulations	4
2.3	Data required for time-domain simulations	5
3	Scenarios in the frequency-domain	7
3.1	Generic “absorber of variable strength”	7
3.2	Axially-travelling perturbations at the velocity of the flow	9
3.3	Fuel assembly vibrations	11
3.4	Control rod vibrations	17
3.5	Core barrel vibrations	19
4	Scenarios in the time-domain	22
4.1	Fuel assembly vibrations	22
4.2	Thermal-hydraulic parameter fluctuations	23
4.3	Combination of fuel assembly vibrations and thermal-hydraulic parameter fluctuations	23
5	Conclusions	23
5.1	Frequency-domain simulations	23
5.2	Time-domain simulations	27
5.2.1	Fuel assembly vibrations	27
5.2.2	Thermal-hydraulic parameter fluctuations	29
5.2.3	Combination of vibrations of a cluster of fuel assemblies and thermal-hydraulic parameter fluctuations	29
6	Bibliography	29

Index of Tables

Table 1:	Description of the considered fuel assembly vibration modes.	11
Table 2:	Description of the considered beam or pendular core barrel vibration modes.	20
Table 3	Summary of the frequency-domain scenarios	25

Table of Figures

Figure 1:	Schematic representation of the decomposition of the spatial domain into nodes.	4
Figure 2:	Labelling of the radial position of the fuel assemblies in a typical PWR core.	6
Figure 3:	Decomposition of the lateral displacement of a vibrating fuel assembly into a x -component and a y -component. The squares represent the fuel assemblies, with the vibrating fuel assembly in grey.	13
Figure 4:	Representation of three neighbouring fuel assemblies with respect to the x -direction.	13
Figure 5:	Representation of three neighbouring fuel assemblies with respect to the y -direction.	15
Figure 6:	Typical core layout showing the boundary between the active core region and the reflector region (represented by the thick black line) and its possible movement.	21
Figure 7.	Steps for estimating the delta gaps of the fuel assemblies (1: main parameters setup,	23
Figure 8.	Location of the vibrating single fuel assemblies.	28
Figure 9.	Location of the central cluster of vibrating fuel assemblies.	28



Abbreviations

APSD	Auto-Power Spectral Density
CORTEX	CORe monitoring Techniques and EXperimental validation and demonstration
CPSD	Cross-Power Spectral Density
PWR	Pressurized Water Reactor
RPV	Reactor Pressure Vessel

Summary

This report summarizes the different scenarios corresponding to the presence of various noise sources in nuclear reactors. The definition of the noise sources and their modelling are carefully detailed, together with the modelling of their effect onto the neutron noise in a nuclear reactor core. Both frequency-domain and time-domain simulation strategies are presented. For the frequency-domain approach, the scenarios include: a generic “absorber of variable strength”, axially-travelling perturbations at the velocity of the flow (due to e.g. fluctuations of the coolant temperature or coolant flow at the inlet of the core), fuel assembly vibrations, control rod vibrations, and core barrel vibrations. For the time-domain approach, the scenarios include: fuel assembly vibrations, inlet coolant temperature fluctuations, inlet coolant flow fluctuations, and their possible combinations.



1 Introduction

The CORTEX project relies on the use of machine learning to unfold from neutron detector readings the possible existence and subsequent characterization of perturbations in a nuclear reactor core. Prior to the unfolding, the machine learning algorithms need to be fed with training data sets, i.e. data for which a known perturbation is assumed and the corresponding induced neutron noise at the location of the detectors is estimated.

The ability of successful unfolding thus heavily relies on covering all possible scenarios in the training data sets.

In this report, the different scenarios to be considered in the training data sets are detailed, together with the assumptions used for modelling the corresponding noise sources. Two types of approaches are retained: frequency-domain simulations and time-domain simulations. For the frequency-domain approach, the scenarios include: a generic “absorber of variable strength”, axially-travelling perturbations at the velocity of the flow (due to e.g. fluctuations of the coolant temperature or coolant flow at the inlet of the core), fuel assembly vibrations, control rod vibrations, and core barrel vibrations. For the time-domain approach, the scenarios include: fuel assembly vibrations, inlet coolant temperature fluctuations, inlet coolant flow fluctuations, and their possible combinations.

The report is structured as follows. In Section 2, the prerequisites for modelling the effect of a noise source onto a nuclear reactor core and for making the results of the simulations directly compatible with the measurement data are first presented. The scenarios in the frequency- and time-domains are thereafter detailed in Sections 3 and 4, respectively. Some conclusions are finally given in Section 5.

2 Prerequisites

Although the scenarios considered in this report are not specific to a given nuclear reactor core, the modelling of a noise source and its effect heavily depends on the core being considered. Moreover, the availability and characteristics of the core instrumentation (both in-core and ex-core) strongly depend on the reactor unit.

2.1 Core instrumentation

The neutron detectors available usually consist of in-core neutron detectors and ex-core neutron detectors. The number and location of those detectors vary considerably from one reactor unit to the other. In addition, the spatial spread of those detectors, both axially and radially, can differ. Finally, the detectors are responding differently to neutrons depending on their energies and on the frequency being considered (some detectors might have a non-negligible delayed component at low frequencies). The knowledge of the reactor transfer function of the neutron detectors with respect to frequency and to the neutron energies is required in order to convert neutron fluxes into detector signals, and vice-versa. Concerning the dependence on energy, most of the neutron detectors are nevertheless mostly sensitive to thermal neutrons.

For the sake of generality in this report, the number, location, axial dimensions and characteristics of the neutron detectors are not explicitly considered. When using the scenarios detailed hereafter for machine learning, care has to be taken in order to guarantee a compatibility between the calculated induced neutron noise and the available detector signals.

2.2 Data required for frequency-domain simulations

The modelling of the effect of a noise source in the frequency-domain is carried out using an extended version of the CORE SIM tool earlier developed at Chalmers University of Technology (Demazière, 2011; Mylonakis et al., 2018).

Considering a three-dimensional reactor core of cylindrical shape in Cartesian geometry, the system is assumed to be made of adjacent homogeneous nodes, as schematically represented in Figure 1. In a Cartesian coordinate system, a node can be represented by the triplet of indexes (I, J, K) , where the indexes I , J , and K refer to the x -, y -, and z -directions, respectively.

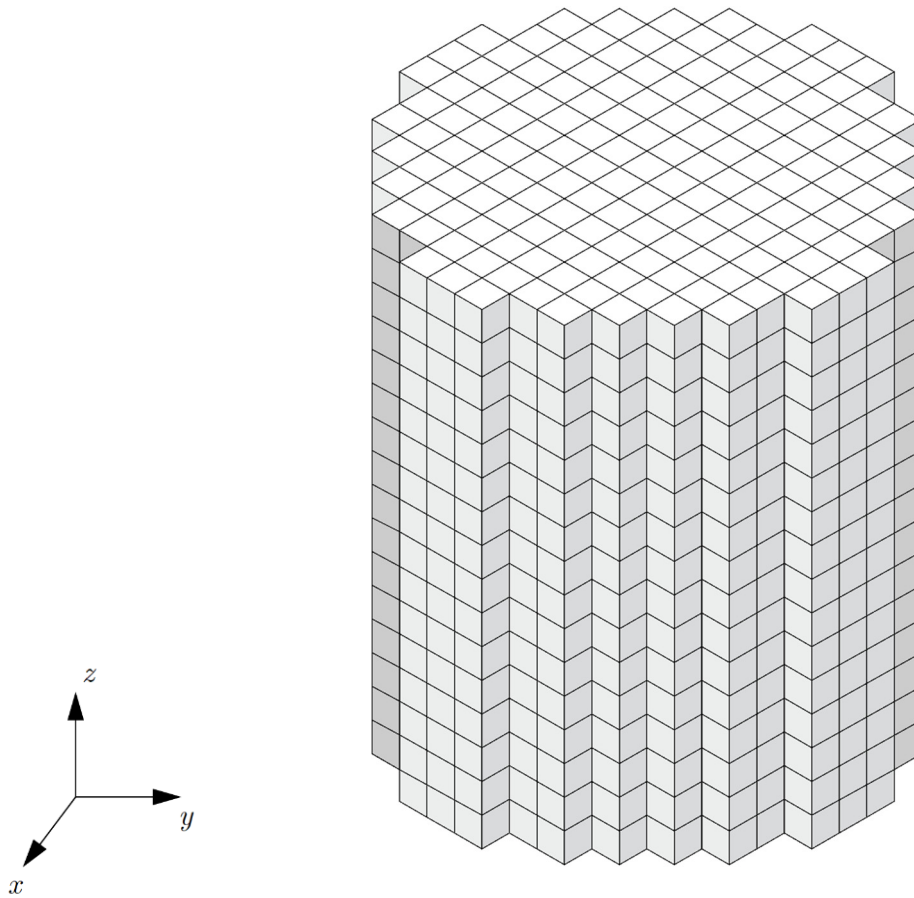


Figure 1: Schematic representation of the decomposition of the spatial domain into nodes.

The modelling of the reactor core in the extended version of CORE SIM requires access to the following data:

- The three-dimensional distributions of the macroscopic data: thermal diffusion coefficient D_1 , fast diffusion coefficients D_2 , the macroscopic removal cross-section Σ_r (defined as the isotropic down-scattering cross-section minus the isotropic up-scattering cross-section weighted with the ratio between the thermal and the fast neutron fluxes), the fast macroscopic absorption cross-section $\Sigma_{a,1}$, the thermal macroscopic absorption cross-section $\Sigma_{a,2}$, ν times the fast macroscopic fission cross-section $\Sigma_{f,1}$ and ν times the

thermal macroscopic fission cross-section $\Sigma_{f,2}$ (with ν being the average number of neutrons released per fission event).

- The three-dimensional distributions of the two-group discontinuity factors: “north” face of a node DFN_1 and DFN_2 for the fast and thermal energy groups, respectively; “south” face of a node DFS_1 and DFS_2 for the fast and thermal energy groups, respectively; “west” face of a node DFW_1 and DFW_2 for the fast and thermal energy groups, respectively; “east” face of a node DFE_1 and DFE_2 for the fast and thermal energy groups, respectively. Careful attention must be paid to the labelling of north, south, west and east for a given node with respect to the chosen directions. In the following, the north, south respectively, faces of a node are found for increasing, decreasing respectively, y values, whereas the east, west respectively, faces of a node are found for increasing, decreasing respectively, x values.
- In case of a uniform mesh, the size Δx , Δy and Δz of an elementary node along the x -, y - and z -directions, respectively. In case of a non-uniform mesh, the one-dimensional distribution of the elementary size Δx , Δy and Δz of the nodes on which these data were created in the x -, y - and z -directions, respectively.
- The point-kinetic data of the core: the effective fraction of delayed neutrons β_{eff} (one group of delayed neutrons), the decay constant of the neutron precursors λ (one group of delayed neutrons), the average neutron speed in the fast group v_1 and the average neutron speed in the thermal group v_2 .

The frequency-domain simulations are carried out at a given angular frequency ω that needs to be specified by the user. In addition, the exact model retained for modelling a given noise source needs to be defined by the user (see Section 3).

2.3 Data required for time-domain simulations

The modelling of the effect of noise sources in the time-domain is carried out using the transient nodal code SIMULATE-3K (Grandi, 2009), along with the 2-D lattice code CASMO-5 (Rhodes et al., 2007) and the 3D steady-state nodal code SIMULATE-3 (Cronin et al., 1998). A typical radial layout of a generic Pressurized Water Reactor (PWR) core is given in Figure 2, together with the conventions used for labelling the positions of the fuel assemblies.

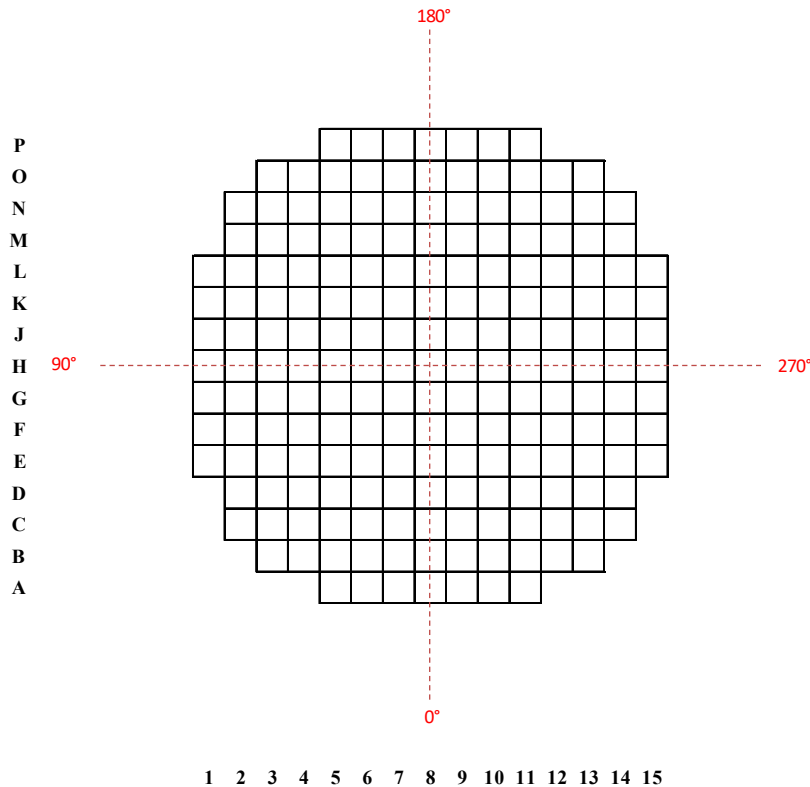


Figure 2: Labelling of the radial position of the fuel assemblies in a typical PWR core.

The CASMO-5 code is used to perform 2-D lattice calculations and generate 2-group homogenized macroscopic cross sections and discontinuity factors for each fuel assembly. These data are then used by both the steady state and transient nodal codes SIMULATE-3 and SIMULATE-3K.

The two-group homogenized macroscopic cross-sections and discontinuity factors are extracted for every relevant node of the core and reflector, from the SIMULATE-3 outputs.

The nodal macroscopic cross sections of interest are:

- ND1: Fast diffusion coefficient.
- ND2: Thermal diffusion coefficient.
- NSA1: Fast macroscopic absorption cross-section.
- NSA2: Thermal macroscopic absorption cross-section.
- NSR1: Macroscopic removal cross-section.
- NNF1: Nu times the fast macroscopic fission cross-section.
- NNF2: Nu times the thermal macroscopic fission cross-section.
- NKN: Kappa over nu.

The discontinuity factors of interest are:

- NF1W: West fast discontinuity factor.
- NF1S: South fast discontinuity factor.
- NF1E: East fast discontinuity factor.
- NF1N: North fast discontinuity factor.
- NF2W: West thermal discontinuity factor.
- NF2S: South thermal discontinuity factor.
- NF2E: East thermal discontinuity factor.
- NF2N: North thermal discontinuity factor.

In addition, the fractions of delayed neutrons (betas) and corresponding decay constants (lamdas) in six groups, the prompt neutron lifetime, and effective fraction of delayed neutrons (betaeff) are also extracted.

3 Scenarios in the frequency-domain

Using the extended version of CORE SIM, the main task of the modeller is to build an adequate model of a noise source for each scenario being considered. It should be mentioned that the spatial mesh used for the calculations can be finer than the one on which the sets of node-homogenized macroscopic data (diffusion coefficients, macroscopic cross-sections, and discontinuity factors) were generated. After building the input noise source, the calculation of the induced neutron noise can be carried out.

3.1 Generic “absorber of variable strength”

The first scenario being considered is a Dirac-like perturbation in point \mathbf{r}_p directly expressed as a perturbation of a macroscopic cross-section. This scenario is particularly important since it constitutes the basis for estimating the reactor Green’s function, as explained hereafter, on which the modelling of the effect of all other types of noise sources can be carried out.

Using two-group diffusion theory and standard notations, the neutron noise in linear theory induced by a Dirac-like perturbation in point \mathbf{r}_p fulfills the following balance equations in the frequency domain (Pázsit and Demazière, 2010):

$$\begin{aligned} & \left\{ \nabla \cdot [\mathbf{D}(\mathbf{r}) \nabla] + \Sigma_{dyn}(\mathbf{r}, \omega) \right\} \times \begin{bmatrix} \delta\phi_1(\mathbf{r}, \omega) \\ \delta\phi_2(\mathbf{r}, \omega) \end{bmatrix} \\ &= \Phi_r(\mathbf{r}) \delta\Sigma_r(\mathbf{r}, \omega) + \Phi_a(\mathbf{r}) \begin{bmatrix} \delta\Sigma_{a,1}(\mathbf{r}, \omega) \\ \delta\Sigma_{a,2}(\mathbf{r}, \omega) \end{bmatrix} + \Phi_f(\mathbf{r}, \omega) \begin{bmatrix} \delta v \Sigma_{f,1}(\mathbf{r}, \omega) \\ \delta v \Sigma_{f,2}(\mathbf{r}, \omega) \end{bmatrix} \end{aligned} \quad (1)$$

where the different matrices and vectors are given as:

$$\mathbf{D}(\mathbf{r}) = \begin{bmatrix} D_{1,0}(\mathbf{r}) & 0 \\ 0 & D_{2,0}(\mathbf{r}) \end{bmatrix} \quad (2)$$

$$\Sigma_{dyn}(\mathbf{r}, \omega) = \begin{bmatrix} -\Sigma_1(\mathbf{r}, \omega) & \frac{v \Sigma_{f,2,0}(\mathbf{r})}{k_{eff}} \left(1 - \frac{i\omega\beta}{i\omega + \lambda} \right) \\ \Sigma_{r,0}(\mathbf{r}) & -\left(\Sigma_{a,2,0}(\mathbf{r}) + \frac{i\omega}{v_2} \right) \end{bmatrix} \quad (3)$$

$$\Phi_r(\mathbf{r}) = \begin{bmatrix} \phi_{1,0}(\mathbf{r}) \\ -\phi_{1,0}(\mathbf{r}) \end{bmatrix} \quad (4)$$

$$\Phi_a(\mathbf{r}) = \begin{bmatrix} \phi_{1,0}(\mathbf{r}) & 0 \\ 0 & \phi_{2,0}(\mathbf{r}) \end{bmatrix} \quad (5)$$

$$\Phi_f(\mathbf{r}, \omega) = \begin{bmatrix} -\frac{\phi_{1,0}(\mathbf{r})}{k_{eff}} \left(1 - \frac{i\omega\beta}{i\omega + \lambda} \right) & -\frac{\phi_{2,0}(\mathbf{r})}{k_{eff}} \left(1 - \frac{i\omega\beta}{i\omega + \lambda} \right) \\ 0 & 0 \end{bmatrix} \quad (6)$$

and where $\Sigma_1(\mathbf{r}, \omega)$ is defined as:

$$\Sigma_1(\mathbf{r}, \omega) = \Sigma_{a,1,0}(\mathbf{r}) + \frac{i\omega}{v_1} + \Sigma_{r,0}(\mathbf{r}) - \frac{v\Sigma_{f,1,0}(\mathbf{r})}{k_{eff}} \left(1 - \frac{i\omega\beta}{i\omega + \lambda} \right) \quad (7)$$

The induced neutron noise $\delta\phi_g(\mathbf{r}, \omega), g = 1, 2$ solution to Eq. (1) can also be obtained in an alternative manner using the so-called Green's function technique. In the most general case, the Green's function in two-group diffusion theory is solution to the following equation:

$$\left[\nabla_{\mathbf{r}} \cdot \left[\mathbf{D}(\mathbf{r}) \nabla_{\mathbf{r}} \right] + \Sigma_{dyn}(\mathbf{r}, \omega) \right] \times \begin{bmatrix} G_{g \rightarrow 1}(\mathbf{r}, \mathbf{r}', \omega) \\ G_{g \rightarrow 2}(\mathbf{r}, \mathbf{r}', \omega) \end{bmatrix} = \begin{bmatrix} \delta(\mathbf{r} - \mathbf{r}') \\ 0 \end{bmatrix}_{g=1} \quad \text{or} \quad \begin{bmatrix} 0 \\ \delta(\mathbf{r} - \mathbf{r}') \end{bmatrix}_{g=2} \quad (8)$$

where the $\nabla_{\mathbf{r}}$ operator is taken with respect to the \mathbf{r} variable and where $\mathbf{D}(\mathbf{r})$ and $\Sigma_{dyn}(\mathbf{r}, \omega)$ are defined in Eqs. (2) and (3), respectively. Multiplying this equation by the transpose of the following vector

$$\begin{bmatrix} S_1(\mathbf{r}', \omega) \\ S_2(\mathbf{r}', \omega) \end{bmatrix} = \Phi_r(\mathbf{r}') \delta\Sigma_r(\mathbf{r}', \omega) + \Phi_a(\mathbf{r}') \begin{bmatrix} \delta\Sigma_{a,1}(\mathbf{r}', \omega) \\ \delta\Sigma_{a,2}(\mathbf{r}', \omega) \end{bmatrix} + \Phi_f(\mathbf{r}', \omega) \begin{bmatrix} \delta v\Sigma_{f,1}(\mathbf{r}', \omega) \\ \delta v\Sigma_{f,2}(\mathbf{r}', \omega) \end{bmatrix} \quad (9)$$

where all the terms on the right hand-side were defined in Eqs. (4)-(6), and integrating over the whole reactor gives Eq. (1), from which one concludes that:

$$\begin{bmatrix} \delta\phi_1(\mathbf{r}, \omega) \\ \delta\phi_2(\mathbf{r}, \omega) \end{bmatrix} = \begin{bmatrix} \int \left[G_{1 \rightarrow 1}(\mathbf{r}, \mathbf{r}', \omega) S_1(\mathbf{r}', \omega) + G_{2 \rightarrow 1}(\mathbf{r}, \mathbf{r}', \omega) S_2(\mathbf{r}', \omega) \right] d^3\mathbf{r}' \\ \int \left[G_{1 \rightarrow 2}(\mathbf{r}, \mathbf{r}', \omega) S_1(\mathbf{r}', \omega) + G_{2 \rightarrow 2}(\mathbf{r}, \mathbf{r}', \omega) S_2(\mathbf{r}', \omega) \right] d^3\mathbf{r}' \end{bmatrix} \quad (10)$$

One notices that the induced neutron noise is given by convolution integrals between the $G_{g \rightarrow g'}(\mathbf{r}, \mathbf{r}', \omega)$ components of the Green's function and the corresponding noise sources $S_g(\mathbf{r}', \omega)$. Evaluating each of the $G_{g \rightarrow g'}(\mathbf{r}, \mathbf{r}', \omega)$ components of the Green's function allows retrieving the induced neutron noise $\delta\phi_{g'}(\mathbf{r}, \omega), g' = 1, 2$, as Eq. (10) demonstrates.

In the case of a generic "absorber of variable strength", a point-like source is considered, i.e. Eq. (8) needs to be solved. Although a point-like source can be generated by point-like perturbations of various macroscopic cross-sections, only the sums of such perturbations in the fast and thermal energy groups, respectively, contribute to the noise source, as Eq. (9) shows, and thus to the induced neutron noise.

For generating the training data sets for machine learning, it is thus sufficient to create data where a point-like source in either the fast energy group or the thermal energy group is present, since only the left-hand side of Eq. (9) is required into Eq. (10). This corresponds to solving Eq. (8) and to calculating the $G_{g \rightarrow g'}(\mathbf{r}, \mathbf{r}', \omega)$ components of the Green's function.

Usually, the neutron noise is measured at a few discrete locations \mathbf{r}_i and the Auto-Power and Cross-Power Spectral Densities are determined accordingly. Using the Wiener-Khinchin theorem, the Auto-Power Spectral Density or APSD of the induced neutron noise in point \mathbf{r}_i for the energy group g also reads as:

$$APSD_{\delta\phi_g}(\mathbf{r}_i, \omega) = \delta\phi_g(\mathbf{r}_i, \omega) \delta\phi_g^*(\mathbf{r}_i, \omega) \quad (11)$$

whereas the Cross-Power Spectral Density or CPSD of the induced neutron noise between point \mathbf{r}_i and point \mathbf{r}_j for the energy group g can be alternatively written as:



$$CPSD_{\delta\phi_g}(\mathbf{r}_i, \mathbf{r}_j, \omega) = \delta\phi_g(\mathbf{r}_i, \omega) \delta\phi_g^*(\mathbf{r}_j, \omega) \quad (12)$$

In Eqs. (11) and (12), the asterisk refers to the complex conjugate. In the case of a point-like source in the energy group g' located in point \mathbf{r}_k , Eqs. (11) and (12) read as:

$$APSD_{\delta\phi_g}(\mathbf{r}_i, \omega) = G_{g' \rightarrow g}(\mathbf{r}_i, \mathbf{r}_k, \omega) G_{g' \rightarrow g}^*(\mathbf{r}_i, \mathbf{r}_k, \omega) \quad (13)$$

and

$$CPSD_{\delta\phi_g}(\mathbf{r}_i, \mathbf{r}_j, \omega) = G_{g' \rightarrow g}(\mathbf{r}_i, \mathbf{r}_k, \omega) G_{g' \rightarrow g}^*(\mathbf{r}_j, \mathbf{r}_k, \omega) \quad (14)$$

The generation of the data thus goes as follows:

1. For every possible location of the noise source \mathbf{r}_k and for all possible locations \mathbf{r}_i of the neutron detectors, estimate the $G_{g \rightarrow g'}(\mathbf{r}_i, \mathbf{r}_k, \omega)$ components of the Green's function.
2. For every possible location of the noise source \mathbf{r}_k , for all possible pairs \mathbf{r}_i and \mathbf{r}_j representing the locations of the neutron detectors, and for a noise source being either fast (i.e. $g = 1$) or thermal (i.e. $g = 2$), estimate the CPSD between the pairs of detectors \mathbf{r}_i and \mathbf{r}_j according to Eq. (14). When $\mathbf{r}_i = \mathbf{r}_j$, the APSD is obtained, as Eq. (14) demonstrates.

The above calculations should be performed in a frequency range of typically 0.1 to 25 Hz.

When using machine learning for unfolding on actual measurement data, the challenge is to:

1. Identify a frequency or a frequency range where a peak in the APSD or CPSD exists.
2. Recover from the measured signal: (a) the position \mathbf{r}_k of the perturbation, and (b) whether the perturbation is a fast (i.e. $g = 1$) or thermal (i.e. $g = 2$) perturbation, or a combination of both. In the case of a combination of a fast and thermal perturbation, the relative weights of the fast versus thermal perturbation should be determined.

It should be mentioned that the generic “absorber of variable strength” as described above might be seen as an artificial perturbation, since this perturbation is directly expressed as fluctuations of macroscopic cross-sections, which themselves cannot be easily related to a “physical” perturbation (as the ones described in the remaining of this Section). Nevertheless, the incentives to estimate the effect of a generic “absorber of variable strength” are twofold:

1. The neutron noise in point \mathbf{r}_i and energy group g' induced by a point-like perturbation in point \mathbf{r}_k and energy group g exactly corresponds to the $G_{g \rightarrow g'}(\mathbf{r}_i, \mathbf{r}_k, \omega)$ component of the Green's function. As will be seen for the other types of noise sources, the induced neutron noise will always be expressed in terms of the Green's function.
2. In case the machine learning-based unfolding fails to identify any of the (more “physical”) scenarios described in the remaining of this Section, being able to estimate the noise source in terms of a fast (i.e. $g = 1$) or thermal (i.e. $g = 2$) perturbation, or a combination of both, as well as its spatial spread is still of very high diagnostic value.

3.2 Axially-travelling perturbations at the velocity of the flow

In this scenario, a perturbation of the coolant is assumed. Although it is more likely that this perturbation is created outside of the core, we will consider, for the sake of generality, that the perturbation can also be created inside the core. Using the system of axes represented in Figure 1, the perturbation is assumed to travel upwards with the coolant along the z -axis at a velocity v . For

simplicity, it is further assumed that the velocity is axially-independent. Furthermore, the effect of the coolant perturbation is supposed to only modify the removal macroscopic cross-section. In the time-domain, the perturbation of the removal cross-section would be expressed as:

$$\delta\Sigma_r(\mathbf{r}, t) \equiv \delta\Sigma_r(x, y, z, t) = \begin{cases} 0, & \text{if } (x, y) \neq (x_0, y_0) \\ 0, & \text{if } (x, y) = (x_0, y_0) \text{ and } z < z_0 \\ \delta\Sigma_r\left(x_0, y_0, z_0, t - \frac{z - z_0}{v}\right), & \text{if } (x, y) = (x_0, y_0) \text{ and } z \geq z_0 \end{cases} \quad (15)$$

or in the frequency-domain as:

$$\delta\Sigma_r(\mathbf{r}, \omega) \equiv \delta\Sigma_r(x, y, z, \omega) = \begin{cases} 0, & \text{if } (x, y) \neq (x_0, y_0) \\ 0, & \text{if } (x, y) = (x_0, y_0) \text{ and } z < z_0 \\ \delta\Sigma_r(x_0, y_0, z_0, \omega) \exp\left[-\frac{i\omega(z - z_0)}{v}\right], & \text{if } (x, y) = (x_0, y_0) \text{ and } z \geq z_0 \end{cases} \quad (16)$$

where (x_0, y_0, z_0) represents the location in the core in which the perturbation is applied, and z corresponds to the axial elevation within the core. The perturbation introduced at (x_0, y_0, z_0) is further assumed to be white, i.e.

$$\delta\Sigma_r(x_0, y_0, z_0, \omega) = 1, \forall \omega \quad (17)$$

For the noise source defined above, Eqs. (9) and (10) simply become:

$$\begin{bmatrix} S_1(\mathbf{r}', \omega) \\ S_2(\mathbf{r}', \omega) \end{bmatrix} = \Phi_r(\mathbf{r}') \delta\Sigma_r(\mathbf{r}', \omega) \quad (18)$$

and

$$\begin{bmatrix} \delta\phi_1(\mathbf{r}, \omega) \\ \delta\phi_2(\mathbf{r}, \omega) \end{bmatrix} = \begin{bmatrix} \int [G_{1 \rightarrow 1}(\mathbf{r}, \mathbf{r}', \omega) S_1(\mathbf{r}', \omega) + G_{2 \rightarrow 1}(\mathbf{r}, \mathbf{r}', \omega) S_2(\mathbf{r}', \omega)] d^3 \mathbf{r}' \\ \int [G_{1 \rightarrow 2}(\mathbf{r}, \mathbf{r}', \omega) S_1(\mathbf{r}', \omega) + G_{2 \rightarrow 2}(\mathbf{r}, \mathbf{r}', \omega) S_2(\mathbf{r}', \omega)] d^3 \mathbf{r}' \end{bmatrix} \quad (19)$$

Using the Wiener-Khinchin theorem, the APSD of the induced neutron noise in point \mathbf{r}_i for the energy group g is given as:

$$APSD_{\delta\phi_g}(\mathbf{r}_i, \omega) = \delta\phi_g(\mathbf{r}_i, \omega) \delta\phi_g^*(\mathbf{r}_i, \omega) \quad (20)$$

whereas the CPSD of the induced neutron noise between point \mathbf{r}_i and point \mathbf{r}_j for the energy group g is given as:

$$CPSD_{\delta\phi_g}(\mathbf{r}_i, \mathbf{r}_j, \omega) = \delta\phi_g(\mathbf{r}_i, \omega) \delta\phi_g^*(\mathbf{r}_j, \omega) \quad (21)$$

The generation of the data thus goes as follows:

1. For every possible location $\mathbf{r}_k \equiv (x_0, y_0, z_0)$ of the introduced perturbation and for all possible locations \mathbf{r}_i of the neutron detectors, estimate the induced neutron noise using Eqs. (18) and (19).
2. For every possible location \mathbf{r}_k of the introduced perturbation, for all possible pairs \mathbf{r}_i and \mathbf{r}_j representing the locations of the neutron detectors, estimate the CPSD between the pairs of detectors \mathbf{r}_i and \mathbf{r}_j according to Eq. (21). When $\mathbf{r}_i = \mathbf{r}_j$, the APSD is obtained, as Eq. (20) demonstrates.

The above calculations should be performed in a frequency range of typically 0.1 to 25 Hz.

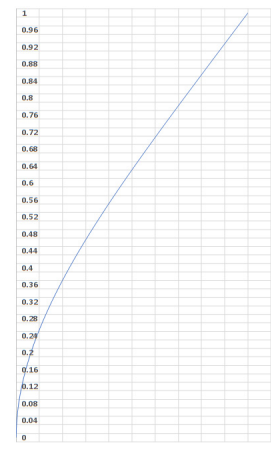
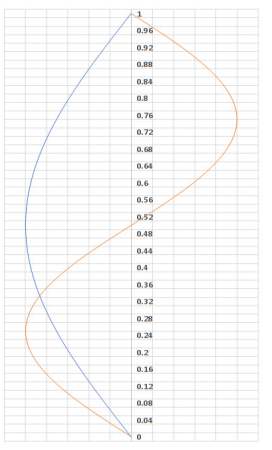
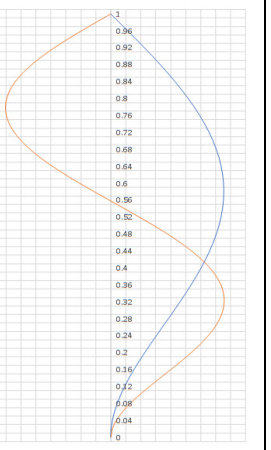
When using machine learning of actual measurement data, the challenge is to:

1. Identify a frequency or a frequency range where a peak in the APSD or CPSD exists.
2. Recover from the measured signal the position \mathbf{r}_k of the introduced perturbation.

3.3 Fuel assembly vibrations

In this scenario, a fuel assembly is assumed to vibrate in the x - and/or y -direction, using the same system of axes as the one represented in Figure 1. Concerning the vibration mode in the axial direction, several possibilities exist, as detailed in Table 1 (Bläsius, 2018).

Table 1: Description of the considered fuel assembly vibration modes.

	Cantilevered beam	Simply supported on both sides	Cantilevered beam and simply supported
Axial shape of the displacement $d(z, t)$ in arbitrary units as a function of the relative core elevation z			
		first mode in blue, second mode in orange	first mode in blue, second mode in orange
Oscillation frequency	Ca. 0.6 – 1.2 Hz	Ca. 0.8 – 4 Hz for the first mode Ca. 5 – 10 Hz for the second mode	Ca. 0.8 – 4 Hz for the first mode Ca. 5 – 10 Hz for the second mode

Analytical expression of the axial shape of the displacement $d(z, t)$	See Eqs. (22), (23) and (24)	See Eqs. (25) and (26)	See Eqs. (27), (28) and (29)
Maximum radial displacement	Ca. 0.4 mm	Ca. 1.5 mm	Ca. 0.1 mm

It will be assumed hereafter that the axial shape of the displacement does not depend on time. This is equivalent to neglecting possible hysteresis in the stiffness behaviour of the fuel assembly, that would otherwise lead to non-harmonic oscillations. Defining H as the core height, the analytical expressions of the axial shape of the displacement are given according to the following equations (Bläsius, 2018):

- For the vibrations of the kind “cantilevered beam” (first mode only):

$$\text{axial shape of } d(z, t) \propto A \left\{ \cos(\kappa_1 z) - \cosh(\kappa_1 z) - \gamma_1 [\sin(\kappa_1 z) - \sinh(\kappa_1 z)] \right\}, \forall t \quad (22)$$

with

$$\kappa_1 = \frac{1.8751}{H} \quad (23)$$

and

$$\gamma_1 = \frac{\cos(\kappa_1 H) + \cosh(\kappa_1 H)}{\sin(\kappa_1 H) + \sinh(\kappa_1 H)} \quad (24)$$

A is a constant to be scaled so that the maximum radial displacement corresponds to the value given in Table 1.

- For the vibrations of the kind “simply supported on both sides”:

$$\text{axial shape of } d(z, t) \propto A \sin(\kappa_\nu z), \forall t \quad (25)$$

with

$$\kappa_\nu = \nu \frac{\pi}{H} \quad (26)$$

The first mode is obtained with $\nu = 1$ and the second mode is obtained with $\nu = 2$. A is a constant to be scaled so that the maximum radial displacement corresponds to the value given in Table 1.

- For the vibrations of the kind “cantilevered beam and simply supported”:

$$\text{axial shape of } d(z, t) \propto A \left\{ \cos(\kappa_\nu z) - \cosh(\kappa_\nu z) - \gamma_\nu [\sin(\kappa_\nu z) - \sinh(\kappa_\nu z)] \right\}, \forall t \quad (27)$$

with

$$\kappa_{\nu=1} = \frac{3.9266}{H} \text{ and } \kappa_{\nu=2} = \frac{7.0686}{H} \quad (28)$$

and

$$\gamma_\nu = \frac{\cos(\kappa_\nu H) + \cosh(\kappa_\nu H)}{\sin(\kappa_\nu H) + \sinh(\kappa_\nu H)} \quad (29)$$

The first mode is obtained with $\nu = 1$ and the second mode is obtained with $\nu = 2$. A is a constant to be scaled so that the maximum radial displacement corresponds to the value given in Table 1.

For the vibrations involving the simply supported types of vibrations, only the first two modes $\nu = 1$ and $\nu = 2$ are considered. Such modes have a larger amplitude in the associated lateral displacements compared to the higher modes. In addition, due to the limited number of neutron detectors along the height of the core, only a limited number of modes can be resolved (Bläsius, 2018).

At a given axial level z , the displacement $d(z, t)$ can be decomposed as a displacement $\varepsilon_x(z, t)$ along the x -direction only and a displacement $\varepsilon_y(z, t)$ along the y -direction only, as depicted in Figure 3.

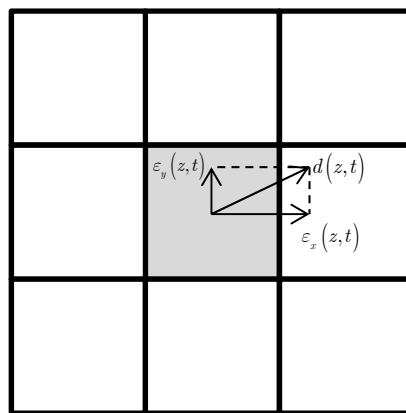


Figure 3: Decomposition of the lateral displacement of a vibrating fuel assembly into a x -component and a y -component. The squares represent the fuel assemblies, with the vibrating fuel assembly in grey.

When considering one direction at a time, the movement of the vibrating fuel assembly can be described in the following manner. Considering e.g. the x -direction and using Figure 4 illustrating three neighbouring fuel assemblies along that direction, the fuel assemblies can be seen as the juxtaposition of three homogeneous regions due to the homogenization of the macroscopic cross-sections.

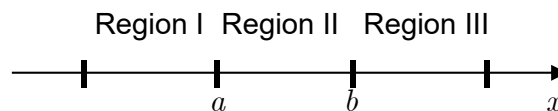


Figure 4: Representation of three neighbouring fuel assemblies with respect to the x -direction.

Considering for the time being Region II and Region III, the spatial distribution of the static macroscopic cross-section for the reaction type α in the energy group g can be represented as:

$$\Sigma_{\alpha,g}^x(x) = [1 - \Theta(x - b)]\Sigma_{\alpha,g,II} + \Theta(x - b)\Sigma_{\alpha,g,III} \quad (30)$$

where $\Theta(x - b)$ is the Heaviside function, i.e.

$$\begin{cases} \Theta(x - b) = 0 & \text{if } x < b \\ \Theta(x - b) = 1 & \text{if } x \geq b \end{cases} \quad (31)$$

In Eq. (30), $\Sigma_{\alpha,g,II}$ represents the macroscopic cross-section of region II, whereas $\Sigma_{\alpha,g,III}$ represents the macroscopic cross-section of region III.

In case of vibrations of the fuel assembly II with respect to III with a displacement $\varepsilon_x(z, t)$, the position of the boundary between regions II and III is time-dependent, and is given as:

$$b(z, t) = b_0 + \varepsilon_x(z, t) \quad (32)$$

where b_0 represents the static position of the boundary between regions II and III. Putting Eq. (32) into Eq. (30), and using a first-order Taylor expansion, one obtains:

$$\begin{aligned} \Sigma_{\alpha,g}^x(x, z, t) \\ = [1 - \Theta(x - b_0)]\Sigma_{\alpha,g,II} + \Theta(x - b_0)\Sigma_{\alpha,g,III} + \varepsilon_x(z, t)\delta(x - b_0)[\Sigma_{\alpha,g,II} - \Sigma_{\alpha,g,III}] \end{aligned} \quad (33)$$

Since the static macroscopic cross-section (i.e. when $\varepsilon_x(z, t) = 0$) is given as:

$$\Sigma_{\alpha,g,0}^x(x) = [1 - \Theta(x - b_0)]\Sigma_{\alpha,g,II} + \Theta(x - b_0)\Sigma_{\alpha,g,III} \quad (34)$$

the noise source corresponding to fluctuations of the position of the boundary between the regions II and III is consequently expressed as:

$$\delta\Sigma_{\alpha,g}^x(x, z, t) = \varepsilon_x(z, t)\delta(x - b_0)[\Sigma_{\alpha,g,II} - \Sigma_{\alpha,g,III}] \quad (35)$$

or in the frequency-domain

$$\delta\Sigma_{\alpha,g}^x(x, z, \omega) = \varepsilon_x(z, \omega)\delta(x - b_0)[\Sigma_{\alpha,g,II} - \Sigma_{\alpha,g,III}] \quad (36)$$

In case of fuel assembly vibrations, the fuel assembly II is displaced by $\varepsilon_x(z, t)$ compared to the equilibrium position b_0 of the boundary between regions II and III and the same displacement $\varepsilon_x(z, t)$ occurs with respect to the equilibrium position a_0 of the boundary between regions I and II. A similar treatment of the vibrations with respect to a_0 as the one presented above with respect to b_0 leads to the following final expression for the noise source in the frequency-domain:

$$\delta\Sigma_{\alpha,g}^x(x, z, \omega) = \varepsilon_x(z, \omega)\delta(x - a_0)[\Sigma_{\alpha,g,I} - \Sigma_{\alpha,g,II}] + \varepsilon_x(z, \omega)\delta(x - b_0)[\Sigma_{\alpha,g,II} - \Sigma_{\alpha,g,III}] \quad (37)$$

As can be seen in the expression above, the noise source corresponding to the vibrations of a fuel assembly with respect to its two neighbours is thus described by two Dirac-like perturbations located at the static boundary of the vibrating fuel assembly.

A similar treatment for the vibrations along the y -direction using the notations introduced in Figure 5 would lead to:

$$\delta\Sigma_{\alpha,g}^y(y, z, \omega) = \varepsilon_y(z, \omega)\delta(y - c_0)[\Sigma_{\alpha,g,IV} - \Sigma_{\alpha,g,II}] + \varepsilon_y(z, \omega)\delta(y - d_0)[\Sigma_{\alpha,g,II} - \Sigma_{\alpha,g,V}] \quad (38)$$

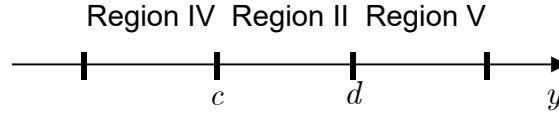


Figure 5: Representation of three neighbouring fuel assemblies with respect to the y -direction.

Due to the axial shapes assumed in Table 1 for the vibration modes, the displacements in the x - and y -directions, respectively, can be factorized as:

$$\varepsilon_x(z, \omega) \equiv \varepsilon_x(\omega) h(z) \quad (39)$$

and

$$\varepsilon_y(z, \omega) \equiv \varepsilon_y(\omega) h(z) \quad (40)$$

so that:

$$d(z, \omega) = h(z) \sqrt{\varepsilon_x^2(\omega) + \varepsilon_y^2(\omega)} \quad (41)$$

As will be seen in the following, the actual radial displacements $\varepsilon_x(\omega)$ and $\varepsilon_y(\omega)$ will only be known in a statistical sense. For the sake of simplicity, we will thus assume that:

$$\sqrt{\varepsilon_x^2(\omega) + \varepsilon_y^2(\omega)} \approx 1 \quad (42)$$

so that:

$$d(z, \omega) \approx h(z) \quad (43)$$

The approximation is further justified by the fact that the analysis of actual neutron noise signals is carried out in relative terms, using e.g. their CPSD. The actual absolute amplitude of the displacement thus becomes irrelevant. It also means that $h(z)$ is given by the right-hand side of Eqs. (22), (25) or (27), depending on the type of perturbation considered.

For the sake of clarity for the following discussions, we rewrite Eqs. (37) and (38) as:

$$\delta\Sigma_{\alpha,g}^x(x, z, \omega) \equiv \varepsilon_x(\omega) \delta\Sigma_{\alpha,g}^x(x, z) \quad (44)$$

and

$$\delta\Sigma_{\alpha,g}^y(y, z, \omega) \equiv \varepsilon_y(\omega) \delta\Sigma_{\alpha,g}^y(y, z) \quad (45)$$

with

$$\delta\Sigma_{\alpha,g}^x(x, z) = h(z) \delta(x - a_0) [\Sigma_{\alpha,g,I} - \Sigma_{\alpha,g,II}] + h(z) \delta(x - b_0) [\Sigma_{\alpha,g,II} - \Sigma_{\alpha,g,III}] \quad (46)$$

and

$$\delta\Sigma_{\alpha,g}^y(y, z) = h(z) \delta(y - c_0) [\Sigma_{\alpha,g,IV} - \Sigma_{\alpha,g,II}] + h(z) \delta(y - d_0) [\Sigma_{\alpha,g,II} - \Sigma_{\alpha,g,V}] \quad (47)$$

Using Eqs. (44)-(47) in Eq. (9), the neutron noise could be evaluated using Eq. (10). Due to the linear property of the neutron noise equation, the neutron noise induced by the vibrations in the x - and y -directions is simply the sum of the neutron noise induced by the vibrations in the x - and y -directions, respectively, i.e.

$$\delta\phi_g(\mathbf{r}, \omega) = \delta\phi_{g,x}(\mathbf{r}, \omega) + \delta\phi_{g,y}(\mathbf{r}, \omega) \quad (48)$$

where $\delta\phi_{g,x}(\mathbf{r}, \omega)$ and $\delta\phi_{g,y}(\mathbf{r}, \omega)$ are given by Eq. (10) taking, respectively, either Eq. (44) or Eq. (45) in the definition of the noise source in Eq. (9).

Due to the factorization into a frequency-dependent part only and a space-dependent part only introduced in Eqs. (44) and (45), one also notices that Eq. (48) can be rewritten as:

$$\delta\phi_g(\mathbf{r}, \omega) = \varepsilon_x(\omega)\delta\varphi_{g,x}(\mathbf{r}, \omega) + \varepsilon_y(\omega)\delta\varphi_{g,y}(\mathbf{r}, \omega) \quad (49)$$

where $\delta\varphi_{g,x}(\mathbf{r}, \omega)$ and $\delta\varphi_{g,y}(\mathbf{r}, \omega)$ are given by Eq. (10) taking, respectively, either Eq. (46) or Eq. (47) in the definition of the noise source in Eq. (9).

Using the Wiener-Khinchin theorem, the APSD of the induced neutron noise in point \mathbf{r}_i for the energy group g is given as:

$$APSD_{\delta\phi_g}(\mathbf{r}_i, \omega) = \delta\phi_g(\mathbf{r}_i, \omega)\delta\phi_g^*(\mathbf{r}_i, \omega) \quad (50)$$

whereas the CPSD of the induced neutron noise between point \mathbf{r}_i and point \mathbf{r}_j for the energy group g is given as:

$$CPSD_{\delta\phi_g}(\mathbf{r}_i, \mathbf{r}_j, \omega) = \delta\phi_g(\mathbf{r}_i, \omega)\delta\phi_g^*(\mathbf{r}_j, \omega) \quad (51)$$

Using Eq. (49) into Eqs. (50) and (51), one obtains, after some algebra:

$$\begin{aligned} & APSD_{\delta\phi_g}(\mathbf{r}_i, \omega) \\ &= S_{xx}(\omega)\|\delta\varphi_{g,x}(\mathbf{r}_i, \omega)\|^2 + 2\text{Re}\left[S_{xy}(\omega)\delta\varphi_{g,x}(\mathbf{r}_i, \omega)\delta\varphi_{g,y}^*(\mathbf{r}_i, \omega)\right] + S_{yy}(\omega)\|\delta\varphi_{g,y}(\mathbf{r}_i, \omega)\|^2 \end{aligned} \quad (52)$$

and

$$\begin{aligned} & CPSD_{\delta\phi_g}(\mathbf{r}_i, \mathbf{r}_j, \omega) \\ &= S_{xx}(\omega)\delta\varphi_{g,x}(\mathbf{r}_i, \omega)\delta\varphi_{g,x}^*(\mathbf{r}_j, \omega) + S_{xy}(\omega)\delta\varphi_{g,x}(\mathbf{r}_i, \omega)\delta\varphi_{g,y}^*(\mathbf{r}_j, \omega) \\ &+ S_{xy}^*(\omega)\delta\varphi_{g,y}(\mathbf{r}_i, \omega)\delta\varphi_{g,x}^*(\mathbf{r}_j, \omega) + S_{yy}(\omega)\delta\varphi_{g,y}(\mathbf{r}_i, \omega)\delta\varphi_{g,y}^*(\mathbf{r}_j, \omega) \end{aligned} \quad (53)$$

with

$$S_{xx}(\omega) = \varepsilon_x(\omega)\varepsilon_x^*(\omega) \quad (54)$$

$$S_{xy}(\omega) = \varepsilon_x(\omega)\varepsilon_y^*(\omega) \quad (55)$$

$$S_{yy}(\omega) = \varepsilon_y(\omega)\varepsilon_y^*(\omega) \quad (56)$$

The model of Pázsit and Glöckler (1984) is finally used to express the vibrations spectra as:

$$S_{xx}(\omega) \propto 1 + k \cos(2\theta) \quad (57)$$

$$S_{xy}(\omega) \propto k \sin(2\theta) \quad (58)$$

$$S_{yy}(\omega) \propto 1 - k \cos(2\theta) \quad (59)$$

In the model given by Eqs. (57)-(59), $k \in [0, 1]$ is the ellipticity or anisotropy of the vibrations and $\theta \in [0, \pi]$ is the preferred direction of vibration. For isotropic vibrations, $k = 0$ whereas for vibrations along a straight line having an angle θ , one has $k = 1$.

The generation of the data thus goes as follows:

1. For every vibration mode given in Table 1, use the corresponding $h(z)$ function and construct $\delta\Sigma_{\alpha,g}^x(x,z)$ and $\delta\Sigma_{\alpha,g}^y(y,z)$ for every possible location of the vibrating fuel assembly using Eqs. (46) and (47), respectively.
2. For every vibration mode given in Table 1, estimate the corresponding neutron noise $\delta\varphi_{g,x}(\mathbf{r},\omega)$ and $\delta\varphi_{g,y}(\mathbf{r},\omega)$ given by Eq. (10) taking, respectively, either Eq. (46) or Eq. (47) in the definition of the noise source in Eq. (9).
3. For every vibration mode given in Table 1, for $k \in [0,1]$ and for $\theta \in [0,\pi]$, estimate the CPSD between the pairs of detectors \mathbf{r}_i and \mathbf{r}_j according to Eq. (53). When $\mathbf{r}_i = \mathbf{r}_j$, the APSD is obtained, as Eq. (52) demonstrates.

The above calculations should be performed in the frequency ranges highlighted in Table 1 for each of the vibration modes modelled.

When using machine learning of actual measurement data, the challenge is to:

1. Identify a frequency or a frequency range where a peak in the APSD or CPSD exists.
2. Identify the vibration mode.
3. Recover from the measured signal the position of the vibrating assembly.
4. Estimate the ellipticity k and the preferred direction θ of vibrations.

3.4 Control rod vibrations

The modelling of control rod vibrations can be relatively easily carried out using the model of Williams (1974) in the so-called weak absorber formulation of Pázsit (1977). The vibration of a control rod is assumed to be described by a one-dimensional structure along the z -direction vibrating perpendicularly to the two-dimensional (x,y) plane, using the system of axes represented in Figure 1. Furthermore, the vibrating rod is assumed to always remain parallel to itself and to have the most significant effect on the thermal macroscopic absorption cross-section. In those conditions, the vibration of the rod will create a perturbation of the thermal absorption cross-section that is represented as:

$$\delta\Sigma_{a,2}(\mathbf{r},t) = \gamma\Theta(z - z_0)\left[\delta(\mathbf{r}_{xy} - \mathbf{r}_{p,xy} - \boldsymbol{\varepsilon}(t)) - \delta(\mathbf{r}_{xy} - \mathbf{r}_{p,xy})\right] \quad (60)$$

where γ is the strength of the perturbation, $\mathbf{r}_{p,xy}$ is the equilibrium position of the rod in the (x,y) plane, $\boldsymbol{\varepsilon}(t)$ is a vector representing the displacement of the rod from its equilibrium position in the (x,y) plane, and z_0 represents the axial elevation at which the rod is inserted (insertion from the top of the core). $\Theta(z - z_0)$ is the Heaviside function, i.e.

$$\begin{cases} \Theta(z - z_0) = 0 & \text{if } z < z_0 \\ \Theta(z - z_0) = 1 & \text{if } z \geq z_0 \end{cases} \quad (61)$$

and allows expressing the fact that a noise source is only defined in the radial plane (x,y) for points having an elevation $z \geq z_0$.

Using a one-term Taylor expansion for Eq. (60), one obtains that:

$$\delta\Sigma_{a,2}(\mathbf{r},t) = -\gamma\Theta(z - z_0)\boldsymbol{\varepsilon}(t) \cdot \delta'(\mathbf{r}_{xy} - \mathbf{r}_{p,xy}) \quad (62)$$

or in the frequency-domain:

$$\delta\Sigma_{a,2}(\mathbf{r},\omega) = -\gamma\Theta(z - z_0)\epsilon(\omega) \cdot \delta'(\mathbf{r}_{xy} - \mathbf{r}_{p,xy}) \quad (63)$$

Since the noise source is expressed as fluctuations of the macroscopic thermal absorption cross-section, this will create a noise source in the thermal group only, as Eq. (9) reveals. Correspondingly, the induced neutron noise becomes, using Eq. (10):

$$\delta\phi_g(\mathbf{r},\omega) = \int G_{2\rightarrow g}(\mathbf{r},\mathbf{r}',\omega)S_2(\mathbf{r}',\omega)d^3\mathbf{r}' \equiv \int \int G_{2\rightarrow g}(\mathbf{r},\mathbf{r}_{xy}',z',\omega)S_2(\mathbf{r}_{xy}',z',\omega)d^2\mathbf{r}_{xy}'dz' \quad (64)$$

Because of the factorization of the noise source into an axial dependence only and a radial dependence only, and taking into account the fact that the noise source $\delta\Sigma_{a,2}(\mathbf{r},\omega)$ is axially homogeneous for $z \geq z_0$ and does not exist otherwise, Eq. (64) can be rewritten as:

$$\delta\phi_g(\mathbf{r},\omega) = -\gamma\epsilon(\omega) \cdot \int \hat{G}_{2\rightarrow g}(\mathbf{r},\mathbf{r}_{xy}',\omega)\delta'(\mathbf{r}_{xy}' - \mathbf{r}_{p,xy})d^2\mathbf{r}_{xy}' \quad (65)$$

where

$$\hat{G}_{2\rightarrow g}(\mathbf{r},\mathbf{r}_{xy}',\omega) = \int G_{2\rightarrow g}(\mathbf{r},\mathbf{r}_{xy}',z',\omega)\Theta(z' - z_0)\phi_{2,0}(\mathbf{r}_{xy}',z')dz' \quad (66)$$

Integrating by parts leads to, assuming that the vibrating rod is not located at the periphery of the system:

$$\delta\phi_g(\mathbf{r},\omega) = -\gamma\epsilon(\omega) \cdot \int \delta(\mathbf{r}_{xy}' - \mathbf{r}_{p,xy})\nabla_{\mathbf{r}_{xy}}\hat{G}_{2\rightarrow g}(\mathbf{r},\mathbf{r}_{xy}',\omega)d^2\mathbf{r}_{xy}' \quad (67)$$

which becomes:

$$\delta\phi_g(\mathbf{r},\omega) = -\gamma\epsilon(\omega) \cdot \nabla_{\mathbf{r}_{p,xy}}\hat{G}_{2\rightarrow g}(\mathbf{r},\mathbf{r}_{p,xy},\omega) \quad (68)$$

For the sake of convenience, we simply rewrite this equation as:

$$\delta\phi_g(\mathbf{r},\omega) = -\gamma\epsilon(\omega) \cdot \delta\varphi_g(\mathbf{r},\omega) \quad (69)$$

with

$$\delta\varphi_g(\mathbf{r},\omega) = \nabla_{\mathbf{r}_{p,xy}}\hat{G}_{2\rightarrow g}(\mathbf{r},\mathbf{r}_{p,xy},\omega) \quad (70)$$

Splitting the $\epsilon(\omega)$ and $\delta\varphi_g(\mathbf{r},\omega)$ vectors into their respective x -and y -contributions, Eq. (70) can be rewritten as:

$$\delta\phi_g(\mathbf{r},\omega) = -\gamma\epsilon_x(\omega)\delta\varphi_{g,x}(\mathbf{r},\omega) - \gamma\epsilon_y(\omega)\delta\varphi_{g,y}(\mathbf{r},\omega) \quad (71)$$

One notices the equivalent form of Eq. (71) compared to Eq. (49). One thus concludes, using Eqs. (52) and (53), that:

$$\begin{aligned} & APSD_{\delta\phi_g}(\mathbf{r}_i,\omega) \\ &= \gamma^2 \left\{ S_{xx}(\omega)\|\delta\varphi_{g,x}(\mathbf{r}_i,\omega)\|^2 + 2\text{Re}[S_{xy}(\omega)\delta\varphi_{g,x}(\mathbf{r}_i,\omega)\delta\varphi_{g,y}^*(\mathbf{r}_i,\omega)] + S_{yy}(\omega)\|\delta\varphi_{g,y}(\mathbf{r}_i,\omega)\|^2 \right\} \end{aligned} \quad (72)$$

and

$$\begin{aligned} & CPSD_{\delta\phi_g}(\mathbf{r}_i,\mathbf{r}_j,\omega) \\ &= \gamma^2 \left\{ \begin{aligned} & S_{xx}(\omega)\delta\varphi_{g,x}(\mathbf{r}_i,\omega)\delta\varphi_{g,x}^*(\mathbf{r}_j,\omega) + S_{xy}(\omega)\delta\varphi_{g,x}(\mathbf{r}_i,\omega)\delta\varphi_{g,y}^*(\mathbf{r}_j,\omega) \\ & + S_{xy}^*(\omega)\delta\varphi_{g,y}(\mathbf{r}_i,\omega)\delta\varphi_{g,x}^*(\mathbf{r}_j,\omega) + S_{yy}(\omega)\delta\varphi_{g,y}(\mathbf{r}_i,\omega)\delta\varphi_{g,y}^*(\mathbf{r}_j,\omega) \end{aligned} \right\} \end{aligned} \quad (73)$$

In addition, the same vibration model as the one given by Eqs. (57)-(59) can be used.

The generation of the data thus goes as follows:

1. For each control rod having for radial location $\mathbf{r}_{p,xy}$ and inserted in the core from the top of to the core elevation z_0 , estimate $\hat{G}_{2 \rightarrow g}(\mathbf{r}, \mathbf{r}'_{xy}, \omega)$ from Eq. (66), and thereafter estimate $\delta\varphi_g(\mathbf{r}, \omega)$ from Eq. (70).
2. For each inserted control rod, estimate the x - and y -contributions of $\delta\varphi_g(\mathbf{r}, \omega)$, i.e. estimate $\delta\varphi_{g,x}(\mathbf{r}, \omega)$ and $\delta\varphi_{g,y}(\mathbf{r}, \omega)$.
3. For each inserted control rod, for $k \in [0, 1]$ and for $\theta \in [0, \pi]$, estimate the CPSD between the pairs of detectors \mathbf{r}_i and \mathbf{r}_j according to Eq. (73). When $\mathbf{r}_i = \mathbf{r}_j$, the APSD is obtained, as Eq. (72) demonstrates.

The above calculations should be performed in the frequency range 0.1-20 Hz.

When using machine learning of actual measurement data, the challenge is to:

1. Identify a frequency or a frequency range where a peak in the APSD or CPSD exists.
2. Recover from the measured signal the position of the vibrating rod.
3. Estimate the ellipticity k and the preferred direction θ of vibrations.

3.5 Core barrel vibrations

Several modes of vibrations are possible for the core barrel. In the following, we will only consider the so-called beam or pendular mode. This mode is particularly challenging since the typical frequency of this mode overlaps with the frequencies of other phenomena for instance related to fuel assembly vibrations. It is thus desirable to be able to differentiate this type of vibrations from others. Other core barrel vibration modes, such as the so-called shell mode, usually take place at higher frequencies.

Two types of beam or pendular motions can occur: the so-called in-phase and out-of-phase modes (Bläsius, 2018). These modes result from the interplay between the oscillations of the Reactor Pressure Vessel (RPV) with respect to the environment and the oscillations of the core barrel with respect to the RPV, to which the core barrel is attached, as illustrated in Table 2. In the in-phase mode, the two oscillators move in the same directions, whereas in the out-of-phase mode, the two oscillators move in opposite directions.

Table 2: Description of the considered beam or pendular core barrel vibration modes.

	In-phase	Out-of-phase
Illustration of the two oscillators		
Oscillation frequency	Ca. 7.0 – 9.0 Hz	Ca. 10.0 – 13.0 Hz
Analytical expression of the axial shape of the displacement $d(z, t)$ of the active core	See Eq. (74)	See Eq. (74)
Maximum radial displacement	Smaller than 60 μm	Ca. 60 μm

For both modes of pendular or beam motions of the core barrel, the axial shape of the displacement of the active core with respect to the environment can be described in the same manner (Bläsius, 2018). Defining H as the core height and by H_0 the distance between the top of the core and the bearing points of the RPV to its environment (which approximately coincide with the bearing points of the core barrel to the RPV), the analytical expression of the axial shape of the displacement is given according to the following equation:

$$\text{axial shape of } d(z, t) \propto A(H + H_0 - z), \forall t \quad (74)$$

A is a constant to be scaled so that the maximum radial displacement corresponds to the value given in Table 2. In western-type PWRs, one has $H_0 \approx 3 \text{ m}$.

From a neutronic viewpoint, the modelling of the pendular mode can be performed much alike the modelling of fuel assembly vibrations described in Section 3.3. Core barrel vibrations can be described as the relative motion of the active fuel core region with respect to the reflector. Core barrel vibrations can thus be seen as a collective movement of all fuel assemblies with respect to the reflector. In terms of modelling and taking advantage of the methodology presented in Section 3.3, the perturbations introduced by core barrel vibrations can be considered as localized perturbations taking place at the boundary between the active core region and the reflector region, depicted by the thicker black line in Figure 6.

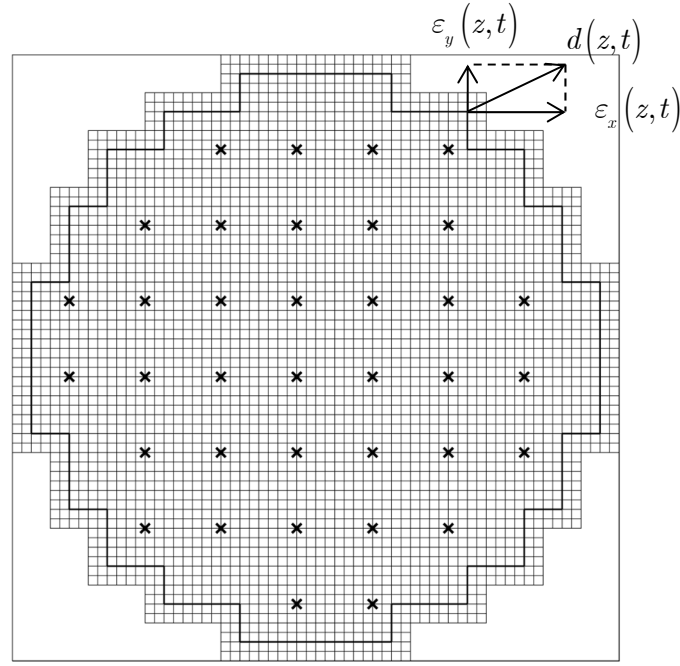


Figure 6: Typical core layout showing the boundary between the active core region and the reflector region (represented by the thick black line) and its possible movement.

The noise source can thus be described by a sum of Dirac-like noise sources along the boundary and decomposed along the x - and y -directions, respectively, as:

$$\delta \Sigma_{\alpha,g}^x(x,z) = h(z) \sum_n \delta(x - x_n) \left[\Sigma_{\alpha,g,x_n^-} - \Sigma_{\alpha,g,x_n^+} \right] \quad (75)$$

and

$$\delta \Sigma_{\alpha,g}^y(y,z) = h(z) \sum_m \delta(y - y_m) \left[\Sigma_{\alpha,g,y_m^-} - \Sigma_{\alpha,g,y_m^+} \right] \quad (76)$$

where the boundary between the active core and the reflector is described by:

- n points in the x -direction located at the abscissa x_n , having for decreasing values of x from x_n a region described by the macroscopic cross-section Σ_{α,g,x_n^-} and having for increasing values of x from x_n a region described by the macroscopic cross-section Σ_{α,g,x_n^+} .
- m points in the y -direction located at the abscissa y_m , having for decreasing values of y from y_m a region described by the macroscopic cross-section Σ_{α,g,y_m^-} and having for increasing values of y from y_m a region described by the macroscopic cross-section Σ_{α,g,y_m^+} .

and where we also assume that:

$$d(z,\omega) \approx h(z) \quad (77)$$

The generation of the data thus goes as follows:

1. Using the function $h(z)$, construct $\delta\Sigma_{\alpha,g}^x(x, z)$ and $\delta\Sigma_{\alpha,g}^y(y, z)$ using Eqs. (75) and (76), respectively.
2. Estimate the corresponding neutron noise $\delta\varphi_{g,x}(\mathbf{r}, \omega)$ and $\delta\varphi_{g,y}(\mathbf{r}, \omega)$ given by Eq. (10) taking, respectively, either Eq. (75) or Eq. (76) in the definition of the noise source given by Eq. (9).
3. For $k \in [0, 1]$ and for $\theta \in [0, \pi]$, estimate the CPSD between the pairs of detectors \mathbf{r}_i and \mathbf{r}_j according to Eq. (53). When $\mathbf{r}_i = \mathbf{r}_j$, the APSD is obtained, as Eq. (52) demonstrates.

The above calculations should be performed in the frequency range corresponding to pendular core barrel vibrations, i.e. 7-13 Hz.

When using machine learning of actual measurement data, the challenge is to:

1. Identify a frequency or a frequency range where a peak in the APSD or CPSD exists.
2. Estimate the ellipticity k and the preferred direction θ of vibrations.

4 Scenarios in the time-domain

Using SIMULATE-3K, many scenarios can be modelled to simulate the impact of various stochastic phenomena on the neutron noise. These include the time-dependent fluctuations of the inlet coolant temperature and flow, as well as the capability to mimic the fuel assembly lateral vibrations in the x- and/or y-direction, as described in the following sections.

4.1 Fuel assembly vibrations

SIMULATE-3K can mimic lateral oscillations of fuel assemblies by activating the vibration model through the KIN.BOW input card. This capability is based on the delta-gap model introduced already in CASMO, which permits creating sets of fuel assembly-wise nodal cross-sections as functions of the delta gap. This approach thus allows modifying in SIMULATE-3K the water gap widths between the fuel assemblies in a time-dependent manner and, therefore, fuel assembly vibrations can be simulated. Complementary to this model, a MATLAB script was developed for the generation of the time-dependent variation of the delta gaps by preserving their values in different directions. Figure 7 summarizes the capabilities of this script to generate the simulated data. First, the user has to define the basic parameters, such as, the time step and the duration of simulation, and the amplitude of the fuel assembly lateral displacement. Then, the choice of the number and the location of vibrating fuel assemblies is given, followed by the selection of the direction of vibration (in x- and/or in y-direction). Afterwards, the type of vibration, e.g. random (white noise) or a sine wave at a preferred frequency value is given. Finally, the user specifies if all the selected fuel assemblies are vibrating identically or randomly between each other. This development extends the flexibility and capabilities of the SIMULATE-3K model and allows the user to impose any kind of lateral fuel assembly vibration.

It should be noted that, so far, the fuel assembly vibration model is restricted to the lateral displacement of the fuel assemblies in which all the axial nodes are displaced simultaneously with the same amplitude. This is rather a simplified approach of the fuel motion. However, more realistic movements will be modelled in the future to include the modes illustrated in Table 1.

Hence, the challenge for the machine learning is to identify the following parameters:

1. Type for disturbance.
2. Frequency of vibrating assemblies.
3. Location of vibrating assemblies.
4. Vibration mode.

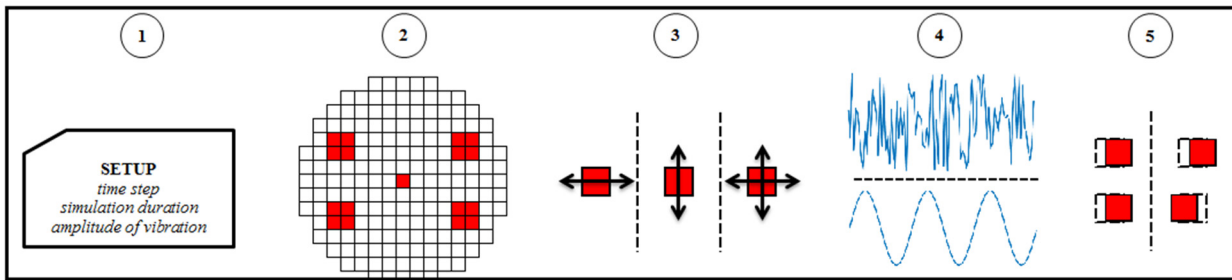


Figure 7. Steps for estimating the delta gaps of the fuel assemblies (1: main parameters setup, 2: selection of vibrating fuel assemblies, 3: direction of vibration, 4: random/sine vibration, 5: synchronized/unsynchronized vibration).

4.2 Thermal-hydraulic parameter fluctuations

SIMULATE-3K has the capability to model the fluctuation of the main thermal-hydraulic parameters, i.e. inlet coolant temperature and flow, and simulate their impact on the neutron noise level. There is a choice in the type of fluctuations, i.e. whether they are random (white noise) or oscillatory (sine wave with a certain frequency). For the generation of these fluctuations, a MATLAB script was developed which generates the SIMULATE-3K input files in order to generate the simulated data. This script allows the user to model random inlet coolant temperature/flow fluctuations, which are either fully synchronized (i.e. identical temperature variation over time in all three loops) or unsynchronized between the coolant loops.

Hence, the challenge for the machine learning of the actual data is to identify the following parameters:

1. Type of disturbance.
2. Frequency or a frequency range of the perturbation.
3. Position of the introduced perturbation.

4.3 Combination of fuel assembly vibrations and thermal-hydraulic parameter fluctuations

The current methodology allows the analyst to combine the perturbations presented in Sections 4.1 and 4.2 and to simulate their effects on the neutron noise level.

The combination of these disturbances represents a more challenging situation for machine learning, since their respective effect on the neutron noise has to be decomposed.

5 Conclusions

This report presented the methods for modelling the perturbations and their effect on the neutron noise for the following scenarios:

- Fuel assembly vibrations (both in the time- and frequency-domain).
- Core barrel vibrations (in the frequency-domain).
- Travelling perturbations with the coolant (both in the time- and frequency-domain).
- Control rod vibrations (in the frequency-domain).
- Absorber of variable strength (in the frequency-domain).

5.1 Frequency-domain simulations

Concerning the frequency-domain simulations, it was demonstrated that the effect due to any of the types of noise sources listed above can be estimated from the knowledge of the group-to-group



Green's functions $G_{g' \rightarrow g}(\mathbf{r}, \mathbf{r}', \omega)$. Those functions actually represent the neutron noise in the energy group g at position \mathbf{r} and angular frequency ω induced by a Dirac-like perturbation in the energy group g' at position \mathbf{r}' at the same frequency.

The determination of the $G_{g' \rightarrow g}(\mathbf{r}, \mathbf{r}', \omega)$ Green's functions thus represents the first step of the calculations to be performed. Such calculations are carried out using the extended version of CORE SIM. Once those transfer functions are available, the effect of the noise sources in each of the scenarios listed above can be determined using the procedures detailed in Section 3 and summarized in Table 3.

Table 3 Summary of the frequency-domain scenarios

Frequency range	Noise source definition	Induced neutron noise	Spectral properties of the induced neutron noise at the locations \mathbf{r}_i of the detectors	Machine learning goals
“Absorber of variable strength”				
0.1 – 25 Hz	Given by $\begin{bmatrix} \delta(\mathbf{r} - \mathbf{r}_k) \\ 0 \end{bmatrix}_{g=1}$ or $\begin{bmatrix} 0 \\ \delta(\mathbf{r} - \mathbf{r}_k) \end{bmatrix}_{g=2}$	Given by $\begin{bmatrix} G_{g \rightarrow 1}(\mathbf{r}, \mathbf{r}_k, \omega) \\ G_{g \rightarrow 2}(\mathbf{r}, \mathbf{r}_k, \omega) \end{bmatrix}$ i.e. solution of Eq. (8)	APSD and CPSD given by Eqs. (13) and (14), respectively	<ol style="list-style-type: none"> 1. Identify this type of noise source 2. Determine the position \mathbf{r}_k of the noise source 3. Determine whether the perturbation is a fast (i.e. $g = 1$) or thermal (i.e. $g = 2$) perturbation
Axially-travelling perturbations at the velocity of the flow				
0.1 – 25 Hz	Given by Eq. (16)	Given by Eqs. (18) and (19)	APSD and CPSD given by Eqs. (20) and (21), respectively	<ol style="list-style-type: none"> 1. Identify this type of noise source 2. Determine the position $\mathbf{r}_k \equiv (x_0, y_0, z_0)$ of the introduced perturbation

Fuel assembly vibrations				
0.6 – 1.2 Hz (cantilevered mode) 0.8 – 4 Hz for first mode (simply supported possibly combined with cantilevered modes) 5.0 – 10.0 Hz for second mode (simply supported possibly combined with cantilevered modes)	For the radial displacement: defined statistically by $k \in [0,1]$ and $\theta \in [0,\pi]$ For the axial displacement: $h(z)$ defined deterministically and given by the right-hand side of Eqs. (22), (25) or (27), depending on the type of perturbation considered, from which the noise sources can be defined according to Eqs. (46) and (47)	Given by $\delta\varphi_{g,x}(\mathbf{r},\omega)$ and $\delta\varphi_{g,y}(\mathbf{r},\omega)$ solution of Eq. (10) taking, respectively, either Eq. (46) or Eq. (47) in the definition of the noise source in Eq. (9)	APSD and CPSD given by Eqs. (50) and (51), respectively	<ol style="list-style-type: none"> 1. Identify this type of noise source 2. Identify the vibration mode. 3. Determine the radial position of the vibrating assembly 4. Estimate the ellipticity k and preferred direction θ of vibrations
Control rod vibrations (only relevant if control rods at radial position $\mathbf{r}_{p,xy}$ are inserted from the top of the core to the core elevation z_0)				
0.1 – 20 Hz	Radial displacement defined statistically by $k \in [0,1]$ and $\theta \in [0,\pi]$	Given by $\delta\varphi_{g,x}(\mathbf{r},\omega)$ and $\delta\varphi_{g,y}(\mathbf{r},\omega)$, being the x - and y - contributions of $\delta\varphi_g(\mathbf{r},\omega)$, itself given by Eq. (70)	APSD and CPSD given by Eqs. (72) and (73), respectively	<ol style="list-style-type: none"> 1. Identify this type of noise source 2. Determine the radial position of the vibrating rod (if several rods are present) 3. Estimate the ellipticity k and preferred direction θ of vibrations

Core barrel vibrations				
7 – 13 Hz	<p>For the radial displacement: defined statistically by</p> $k \in [0,1] \text{ and } \theta \in [0, \pi]$ <p>For the axial displacement: $h(z)$ defined deterministically and given by the right-hand side of Eq. (74), from which the noise sources can be defined according to Eqs. (75) and (76)</p>	<p>Given by $\delta\varphi_{g,x}(\mathbf{r}, \omega)$ and $\delta\varphi_{g,y}(\mathbf{r}, \omega)$ solution of Eq. (10) taking, respectively, either Eq. (75) or Eq. (76) in the definition of the noise source in Eq. (9)</p>	<p>APSD and CPSD given by Eqs. (50) and (51), respectively</p>	<ol style="list-style-type: none"> 1. Identify this type of noise source 2. Estimate the ellipticity k and preferred direction θ of vibrations

It should be emphasized that several noise sources might coexist at the same time. This explains why the first task of the machine learning algorithms is to correctly identify the type(s) of scenario(s) being present in the neutron noise signals. Because of the linear property of the neutron transport operator and of the neglect of the second-order terms in the balance equations for the neutron noise, the induced neutron noise is simply the sum of the neutron noise induced by each of the individual noise source contributions. Furthermore, the actual amplitude of each of the noise sources in each of the scenarios cannot be known in absolute terms, i.e. the actual displacement amplitude of the components is not known. For machine learning, this means that only the relative spatial distribution of the neutron noise between two detectors represents the relevant information to be used.

5.2 Time-domain simulations

5.2.1 Fuel assembly vibrations

Many scenarios have been simulated whether by vibrating a single fuel assembly or a cluster of fuel assemblies.

Vibrations of single fuel assemblies in x-direction

For each scenario of this category, only one fuel assembly is vibrating and only in one direction (in the x-direction). Depending on the analysed scenario, a vibrating fuel assembly is located in the core location E4 (southwest), or E12 (southeast), or L4 (northwest), or L12 (northeast), as shown in Figure 8 (the red squares indicate the location of the vibrating fuel assemblies). The amplitude of vibration is selected to be 1.1 mm, 0.825 mm, 0.55 mm, or 0.275 mm. The fuel assembly is modelled to vibrate by following a white noise signal (random displacement) or a sine wave function with a nominal frequency of 1.5 Hz.

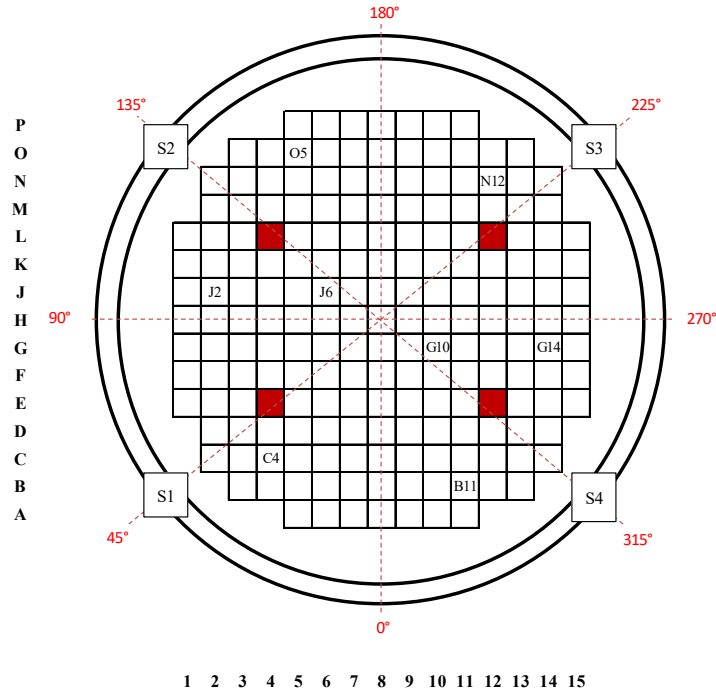


Figure 8. Location of the vibrating single fuel assemblies.

Vibrations of a cluster of fuel assemblies

For each scenario of this category, a central cluster of 5x5 fuel assemblies is vibrating, as shown in Figure 9 (the red squares indicate the location of the vibrating fuel assemblies). The vibration can be performed in three different possible directions, i.e. x-, y- and xy-direction. The amplitude of vibrations is selected to be 1 mm and 0.5 mm. The cluster of fuel assemblies is modelled to vibrate by following a white noise signal (random displacement) or a sine wave function with nominal frequency of 1.5 Hz.

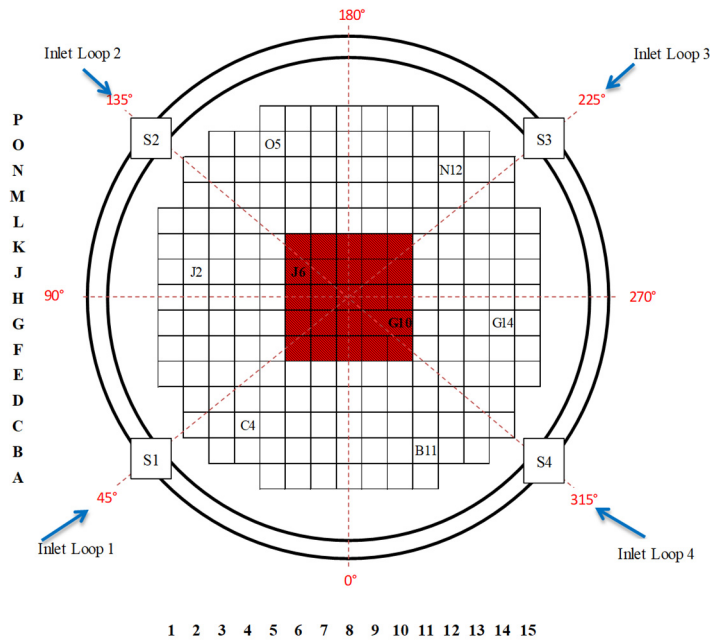


Figure 9. Location of the central cluster of vibrating fuel assemblies.



5.2.2 Thermal-hydraulic parameter fluctuations

In this category, the scenarios are based on fluctuating the inlet coolant temperature or/and inlet coolant flow in a random manner (white noise) with a fluctuation amplitude of 1°C and 1%, respectively, with respect to the mean value.

5.2.3 Combination of vibrations of a cluster of fuel assemblies and thermal-hydraulic parameter fluctuations

In this category, the scenarios are based on the combination of the vibrations of the 5x5 central fuel assembly cluster with the fluctuations of the inlet coolant temperature or/and inlet coolant flow. The vibrations of the cluster are performed in the x-direction, while their amplitude is selected to be 1 mm or 0.5 mm. The fuel assembly cluster is modelled to vibrate by following a white noise signal (random displacement) or a sine wave function with nominal frequency of 1.5 Hz. The thermal-hydraulic fluctuations are following a white noise signal with amplitudes of 1°C and 1% for the inlet coolant temperature and flow, respectively.

6 Bibliography

Bläsius, C. (2018). Private communication. Gesellschaft für Anlagen- und Reaktorsicherheit (GRS) gGmbH.

Cronin, J.T., Smith, K.S., Van der Planck, D.M. (1998). SIMULATE-3 methodology – Advanced three-dimensional two-group reactor analysis code. SOA-980 18, Revision 0, Studsvik.

Demazière, C. (2011). CORE SIM: A multi-purpose neutronic tool for research and education. *Annals of Nuclear Energy*, 38 (12), 2698-2718. <https://doi.org/10.1016/j.anucene.2011.06.010>

Grandi, G. (2009). SIMULATE-3K – Models and methodology. SSP-98/13 Rev.6, Studsvik Scandpower.

Mylonakis A.G., Vinai P., Demazière C. (2018), Neutron noise modelling for nuclear reactor core diagnostics. In: Proc. 27th Symposium of the Hellenic Nuclear Physics Society, June 8-9, 2018, Athens, Greece.

Pázsit, I., 1977. Investigation of the space-dependent noise induced by a vibrating absorber. *Atomkernenergie*, 30, 29-35.

Pázsit, I., & Demazière, C. (2010). Noise techniques in nuclear systems. In D. Cacuci (Ed.), *Handbook of Nuclear Engineering* (pp. 1629-1737). New York, NY, USA: Springer. https://doi.org/10.1007/978-0-387-98149-9_14

Pázsit, I., & Glöckler, O. (1984). On the neutron noise diagnostics of pressurized water reactor control rod vibrations II. Stochastic vibrations. *Nuclear Science and Engineering*, 88, 77-87. <https://doi.org/10.13182/NSE84-4>

Rhodes, J., Smith, K., Lee, D. (2007). CASMO-5/CASMO-5M – A fuel assembly burnup program: Methodology manual. SSP-080405, Revision 0, Studsvik Scandpower.



Williams, M.M.R., 1974. Random processes in nuclear reactors. Oxford, UK: Pergamon Press.
<https://doi.org/10.1016/C2013-0-05660-5>